Supporting Information: Molecular Origin of Distinct Hydration Dynamics in Double Helical DNA and RNA Sequences

Elisa Frezza,[†] Damien Laage,[‡] and Elise Duboué-Dijon*[,¶]

[†]*Université Paris Cité, CiTCoM, Paris, France*

[‡]*PASTEUR, Department of Chemistry, École Normale Supérieure-PSL, Sorbonne Université, CNRS, Paris 75005, France*

[¶]*Université Paris Cité, CNRS, Laboratoire de Biochimie Théorique, 13 rue Pierre et Marie Curie, 75005, Paris, France*

E-mail: elise.duboue-dijon@cnrs.fr

Computational details

Molecular Dynamics simulations

For dsDNA and dsRNA, based on the sequence the structure was energy optimized using the internal/helicoidal variable modelling JUMNA[S1] with the AMBER parm99 force field with the BSC0 modifications[S2] and a Generalized Born continuum solvent model using the parametrization of Tsui and Case,[S3] which comprises added salt effects via a Debye-Hückel term. Standard parameter for B- and A- form was used.

Molecular dynamics simulations were performed with the GROMACS 5 package,[S4–S7] using the Amber force field for nucleic acids in its parmbsc0 version[S2] with χ_{OL3} modifications for RNA molecules.[S8] The double-stranded nucleic acid was placed in a cubic box and solvated with SPC/E water molecules[S9] to a depth of at least 15Å. The SPC/E water model has been shown to give a correct description of water dynamics at ambient conditions[S10] and previous work on DNA hydration dynamics with SPC/E computed slowdowns in very good agreement with NMR measurements.[S11] In addition, the 4-point model TIP4P/2005 and SPC/E have been shown to give very consistent results regarding the conformation of RNA duplexes.[S12] The simulation box was neutralized with potassium cations and then K^+Cl^- ion pairs[S13] were added to reach a physiological salt concentration of 0.15 M. Long-range electrostatic interactions were treated using the particle mesh Ewald method[S14,S15] with a real-space cutoff of 10 Å. The hydrogen bond lengths were restrained using P-LINCS,[S16] allowing a time step of 1 fs. Translational movement of the solute was removed every 1000 steps to avoid any kinetic energy build-up.[S17]

Before the MD production, we carried out the energy minimization using potential restraints on the heavy atoms (constant equal to 1,000 kJ mol^{-1} nm^{-2}) and an equilibration step. During the first step of the equilibration (2 ns) the positional restraints are released. During the first 500 ps, the Bussi velocity-rescaling thermostat ($\tau_T = 0.1$ ps)[S18] and Berendsen pressure coupling ($\tau_P = 0.5$ ps)[S19] were used. The last part of the first step of the

equilibration was carried out in an NTP ensemble at a temperature held at 300 K and a pressure held constant at 1 bar using the Bussi velocity-rescaling thermostat ($\tau_T = 0.1$ ps)[S18] and the Parrinello-Rahman barostat ($\tau_P = 0.5$ ps).[S20] The second step of the equilibration (2 ns) was carried an NTP ensemble at a temperature held at 300 K using the Bussi velocity-rescaling thermostat ($\tau_T = 0.1$ ps).[S18] The production part was performed using the same ensemble of the second step of the equilibration. The length of each simulations was at 100 ns with a high printing frequency (every 250 fs).

Input and parameter files are shared in the SI-files.tar.gz supporting information folder, as well as in a Zenodo public repository.[S21]

Nucleic acid structural analyses

Helical, backbone and groove parameters of nucleic acid structures

The conformational analysis of dsDNA was performed using Curves+,[S22] which provides a full set of helical, backbone and groove geometry parameters. A snapshot representative of typical B-DNA and A-RNA helices conformations is provided in Figure S1.

Parameters are grouped into five sets: (i) intra-base pair (shear, stretch, stagger, buckle, propeller, opening); (ii) BP-axis (Xdisp, Ydisp, inclination and tip); (iii) inter-BP (shift, slide, rise, tilt, roll, twist); (iv) backbone (in the 5' $\rightarrow$ 3' direction for each nucleotide, α P-O5', β O5'-C5', γ C5'-C4', δ C4'-C3', ϵ C3'-O3', ζ O3'-P, the glycosidic angle χ C1'-N1/N9 and the sugar pucker phase and amplitude); (v) groove (minor and major groove widths and depths). All Curves+ parameters are output in a file containing a single record for each snapshot in each oligomer, which allowed us to perform further statistical analysis using Canal.[S22,S24]

Angle analysis

First, we centered the simulation box on the biomolecule and at the center (0,0,0). Then for each snapshot, we computed the inertia tensor to determine the principal component axes

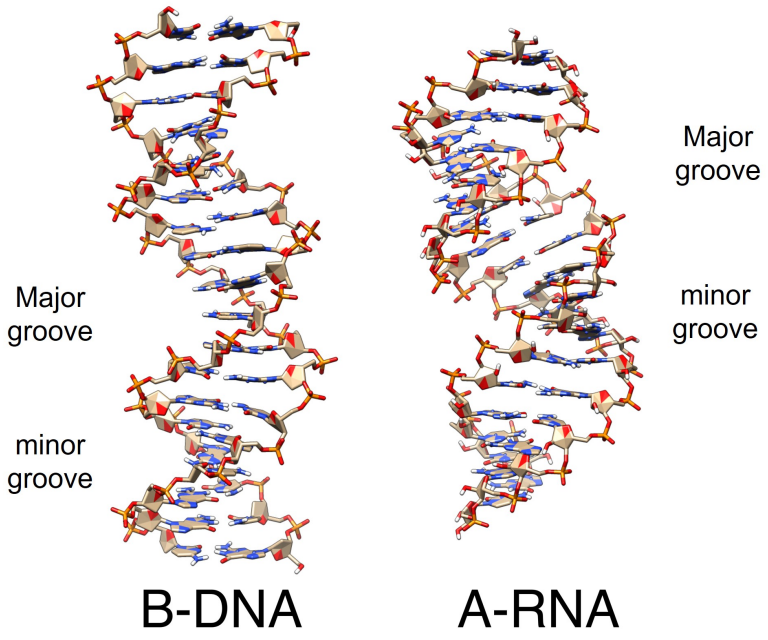

Figure S1: Typical conformations of DNA and RNA double helices.This snapshot was prepared using the VMD software.[S23]

using the package *Orient* in VMD (see Figure S2).[S23] Each snapshot was then aligned along the principal z-axis. To analyze the orientation of the phosphate group, we defined three angles as illustrated in main manuscript (Figure 4): α_{OP2}, α_{P_S} and α_{P_R}. The angle α_{OP2} is defined as:

$$\alpha_{OP2} = \arccos\left(|\hat{\mathbf{e}}_z \cdot \hat{\mathbf{e}}_{PO2}|\right) \tag{1}$$

where $\hat{\mathbf{e}}_z$ is the unit vector parallel to the principal z-axis and $\hat{\mathbf{e}}_{PO2}$ is the unit vector parallel to the bisector of angle formed by the atoms OP_S, P and OP_R. The individual orientations of the O_S and O_R with respect to the groove are then monitored through the α_{P_S} and α_{P_R} angles defined as:

$$\alpha_{Pi} = \arccos\left(-\hat{\mathbf{e}}_{xy} \cdot \hat{\mathbf{e}}_{Pi}\right) \tag{2}$$

where $\hat{\mathbf{e}}_{xy}$ is the unit vector parallel to the projection of the atom P on the plane (x, y) and $z = z_P$ and $\hat{\mathbf{e}}_{Pi}$ is the unit vector parallel to bond P-OP_i with i equal to 1 or 2. These angles quantify if the phosphate oxygen atoms point inside ($\alpha_{Pi} < 90^\circ$) or outside the groove. For

each angle, we computed its time series, the average and the standard deviation using the same definition reported in.[S25]

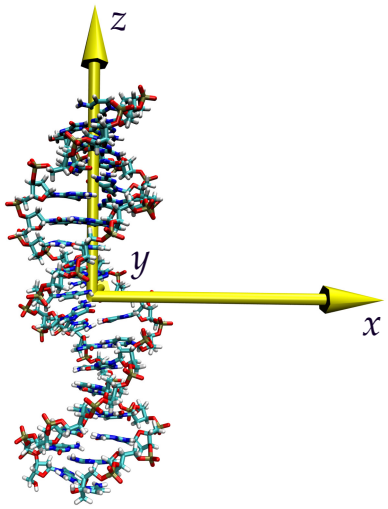

Figure S2: Principal axes for the double stranded NA.

In DNA duplexes, O_R always points outside the groove, when in RNA duplexes O_S points outside the groove (average values of α_{P_S} between 130.9° and 142.7°) and O_R is strongly pointing towards the inside of the groove, with very small values of α_{P_R} (average between 20.7° and 55.1° for GGGG-RNA).

Hydration shell dynamics

Site-resolved definition of the hydration shell. The hydration shell definition and the spatially resolved analysis of hydration shell dynamics follow the same methodology as that used in previous work.[S11,S26,S27] The hydration shell is defined to include all the water OH groups that are H-bonded to or within hydrophobic cutoff of the dodecamer surface. Each water OH group within the shell is then assigned to a nucleic acid surface site using the following procedure. The dodecamer surface is divided into H-bond acceptor, H-bond donor and hydrophobic sites. Hydrophobic radii and H-bond geometric criteria are determined for each site from the first minimum of the radial distribution functions between the water

oxygen atom and the relevant DNA or RNA atom. Typical resulting criteria are $R_{COw} < 4.5$ Å for a hydrophobic site, and $R_{da} < 3.5$ Å $R_{ah} < 2.5$ Å and $\theta_{hda} < 30°$, for a H-bond, where C is a nucleic acid carbon atom, O is a water oxygen atom, a is a H-bond acceptor atom (typically, oxygen or nitrogen atom on the nucleic acid), d a H-bond donor atom (typically, the hydrogen atom of NH or OH groups on DNA or RNA), and h a nucleic acid or water hydrogen atom. All geometric criteria employed for sites definition are listed in the site definitions files provided in the SI-files folder.

Water reorientation dynamics. Hydration water reorientation dynamics is quantified with the reorientation time correlation function (TCF) $C_{reor}(t)$ which probes the reorientation of water OH bond:

$$C_{reor}(t) = \langle P_2 \left[\mathbf{u}(0) \cdot \mathbf{u}(t) \right] \rangle \tag{3}$$

where $\mathbf{u}(t)$ is the vector direction of the water OH bond at time t and P_2 is the second-order Legendre polynomial.

The associated reorientation time τ_{reor}, measurable by NMR, is obtained as by numerical integration of the reorientation TCF:

$$\tau_{reor} = \int_0^\infty C_{reor}(t) \mathrm{d}t \tag{4}$$

The retardation factor with respect to the bulk, ρ_{reor} is then defined as:

$$\rho_{reor} = \frac{\rho_{reor}^{shell}}{\rho_{reor}^{bulk}}, \text{ where } \quad \tau_{reor}^{bulk} = 1.7 \text{ ps} \tag{5}$$

H-bond dynamics. Jump H-bond exchanges can be viewed as chemical reactions where an original H-bond is broken and a new one is formed.[S28,S29] The jump dynamics are probed by the probability for an OH group initially stably H-bonded to a given acceptor I not to have jumped to form a new stable H-bond with any final acceptor F after a given delay. The

jump correlation function $C_j(t)$ is defined by

$$C_j(t) = 1 - \{n_I(0)n_F(t)\} \tag{6}$$

where $n_{I,F}(t) = 1$ if the OH bond forms a stable H-bond at time t respectively with the *I,F* acceptors (as guaranteed by absorbing boundary conditions), and $n_{I,F}(t) = 0$ otherwise.[S30] The jump time is then obtained by time integration of C_j for each DNA site:

$$\tau_j = \int_0^\infty C_j(t)\mathrm{d}t. \tag{7}$$

The retardation factor with respect to the bulk, ρ_{jump} is then defined as:

$$\rho_{jump} = \frac{\rho_{jump}^{shell}}{\rho_{jump}^{bulk}}, \text{ where } \quad \tau_{jump}^{bulk} = 2.5 \text{ ps} \tag{8}$$

The assignment of water molecules to a nucleic acid site and the subsequent calculation of site-resolved jump TCFs is performed with a home-made Fotran code with openMP parallelization, available as a public GitLab repository.[S31] The jump TCF is calculated up to 200 ps for each site. If the decay is not completed at this point, the integrated jump time includes mono-exponential extrapolation of the jump TCF decay at long times.

Estimation of error bars. To assess convergence of these dynamical properties (jump and reorientation) at a single-site level, we estimated error bars by dividing our trajectories in 4 blocks and computing the jump and reorientation times independently on each block. The error bar is then estimated as the standard deviation over these 4 blocks. The jump and reorientation times for each biomolecular site, together with the associated error bars, are summarized in the files "summary_integtime_jump.dat" and "summary_integtime_reor.dat" provided in the folder SI-files.zip, the definition of the sites being written in "site_details.out".

The computed error bars are below 1 ps, even for the slowest sites, and much smaller

for fast hydration sites. Typically, for important sites discussed in the manuscript, in RNA-GGGG, the average jump time is 4.8 ± 0.1 ps for 2′OH sites ; 28.9 ± 1.0 ps for O_R sites, and 16.6 ± 1.3 ps for O_S sites. In DNA-GGGG, the average jump time is 15.6 ± 0.3 ps for O_R sites, 18.9 ± 0.5 ps for O_S sites, and 24.4 ± 1.0 ps for the slowest O2(C) sites on the bases.

Extended jump model

TSEV The Transition-State Excluded Volume (TSEV) retardation factor, ρ_{TSEV}, quantifies the entropic slowdown induced in water dynamics by the presence of a nearby solute which blocks the approach of the new acceptor.[S32] It is numerically estimated for each site by computing, for each water molecule assigned to this site, the fraction f of possible jump transition state locations for a new water H-bond acceptor that overlaps the exclusion sphere (defined for each type of atom based on radial distribution functions between the considered atom type and water) of any of the heavy atoms of the DNA dodecamer and/or ions:

$$\rho_{TSEV} = \frac{1}{1-f} \,. \tag{9}$$

Numerical estimation of the TSEV factor at each site is performed with a home-made Fortran code using the formula described elsewhere.[S32] The list of exclusion radii used for each atom types is given in the files exclvolfile_DNA.inp and exclvolfile_RNA.inp provided in the folder SI-files.

TSHB The Transition-State Hydrogen-Bond factor, ρ_{TSHB},[S33] quantifies the impact of a change in the free energy cost to elongate the initial H-bond on water reorientation dynamics. This factor is primarily enthalpic (strong H-bonds slow down water dynamics), but also has a non negligeable entropic contribution: the environment (e.g. presence of a nearby biomolecular interface) can make the elongation of the initial H-bond more costly. ρ_{TSHB} is numerically estimated for each biomolecular site from radial distribution functions as:

$$\rho_{TSHB} = \exp \frac{\Delta G^{\ddagger}_{\text{site}} - \Delta G^{\ddagger}_{\text{bulk}}}{RT} = \frac{g_{\text{bulk}}(R^{\ddagger}) g_{\text{site}}(R_{eq})}{g_{\text{bulk}}(R_{eq}) g_{\text{site}}(R^{\ddagger})}, \tag{10}$$

where $\Delta G^{\ddagger}$ is the free energy cost to elongate the initial H-bond to its transition state value $R^{\ddagger}$ (taken for simplicity as $R^{\ddagger} = 3.3\,\text{Å}$), and g_{OP-Ow} is the radial distribution function, corrected for excluded volume (which here has very minor impact), between the phosphate oxygen atom of the studied site and water oxygen.

Additional results

Structural analyses

Groove structure analysis

Table S1 summarizes the average values of the minor and major groove parameters (width and depth) of A-RNA and B-DNA double helices for both GGGG and CGCG 18-mers. For the investigated ds-RNAs, the minor groove width is on average equal to 9.8 Å and 10.1 Å, for GGGG and CGCG respectively, while it is significantly smaller (7.9 Å and 7.2 Å) for the analogous DNA helices. An opposite trend is observed for the depth of the minor groove, on average equal to 0.7 Å and 1.0 Å for GGGG-RNA and CGCG-RNA respectively, and much deeper in ds-DNAs, with an average depth of 3.5 Å and 4.6 Å for GGGG and CGCG respectively. As expected, RNA major groove is much more narrow —average width of 6.3 Å and 5.3 Å for GGGG-RNA and CGCG-RNA respectively—and deeper—average depth of 10.8 Å (GGGG-RNA) and 9.9 Å (CGCG-RNA)—than the minor groove while the opposite is true in DNA (see Figures S3 and S4.).

Table S1: Average groove width and depth for A-RNA and B-DNA GGGG and CGCG sequences.

	A-RNA		B-DNA	
	GGGG	CGCG	GGGG	CGCG
minor groove width (Å)	9.8	10.1	7.9	7.2
minor groove depth (Å)	0.7	1.0	3.5	4.6
Major groove width (Å)	6.3	5.3	12.4	11.1
Major groove depth (Å)	10.8	9.9	10.1	6.1

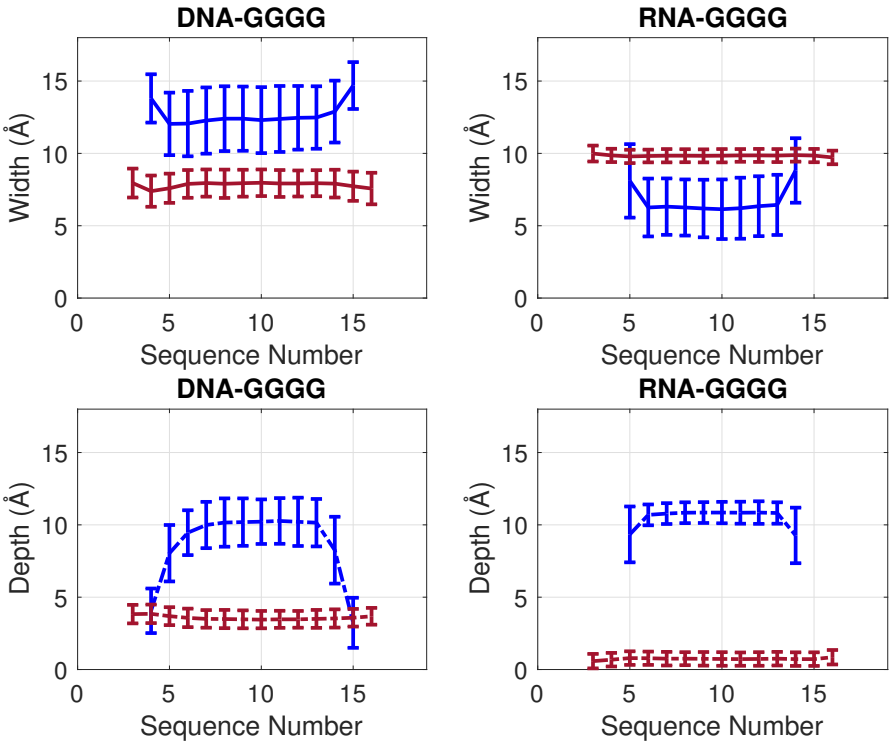

Figure S3: DNA groove dimensions (Å), width (top) and depth (bottom), obtained for DNA-GGGG (left) and RNA-GGGG sequences (right). Red: minor groove. Blue: major groove. The plots were prepared using MATLAB.[S34]

Additional structural analysis of phosphate orientation in CGCG DNA and RNA sequences

Figures S5 and S6 quantify the different phosphate orientations in the DNA and RNA CGCG double helices. They are the analogous for CGCG of Fig. 2 in the main text for GGGG.

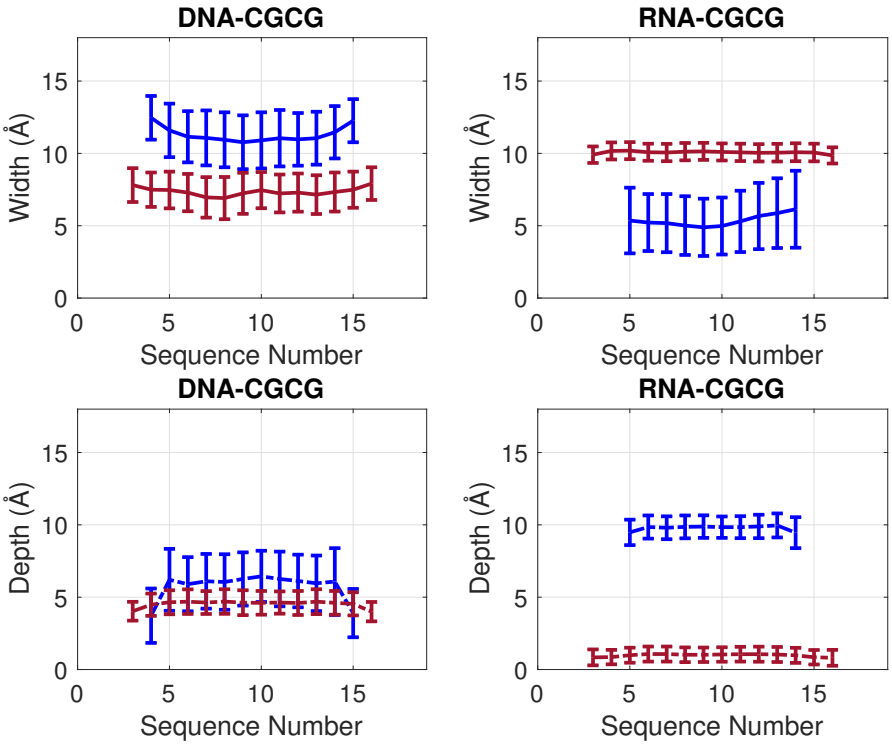

Figure S4: DNA groove dimensions (Å), width (top) and depth (bottom), obtained for DNA-CGCG (left) and RNA-CGCG sequences (right). Red: minor groove. Blue: major groove. The plots were prepared using MATLAB.[S34]

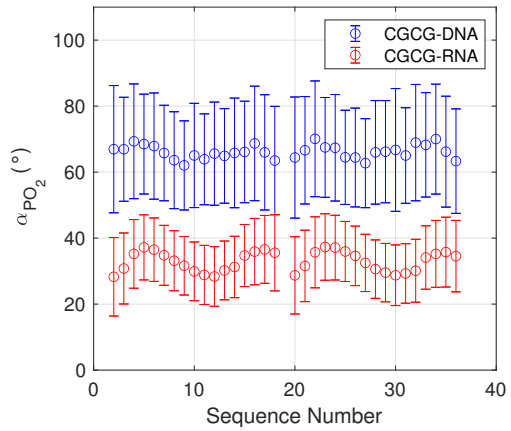

Figure S5: Average and standard deviation of the angle α_{OP2} for the sequence CGCG. Blue: DNA. Red: RNA.

Jump time distributions

The overall jump time distributions for the DNA and RNA GGGG and CGCG sequences are presented in Figure S7.

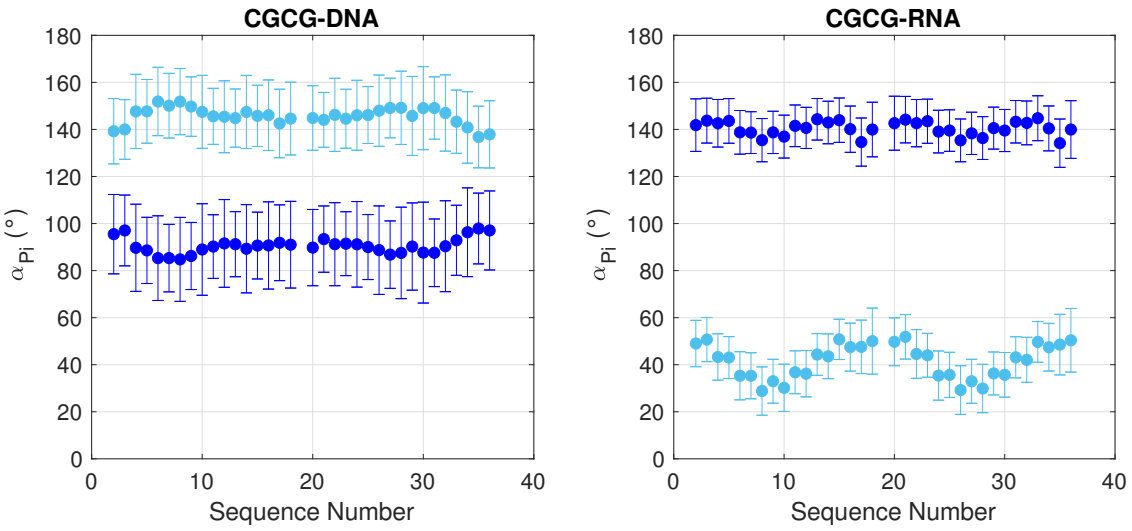

Figure S6: Average and standard deviation of the angle α_{P_i} for the sequence CGCG. Left: DNA. Right: RNA. Light blue: angle α_{P_S}. Blue: angle α_{P_R}.

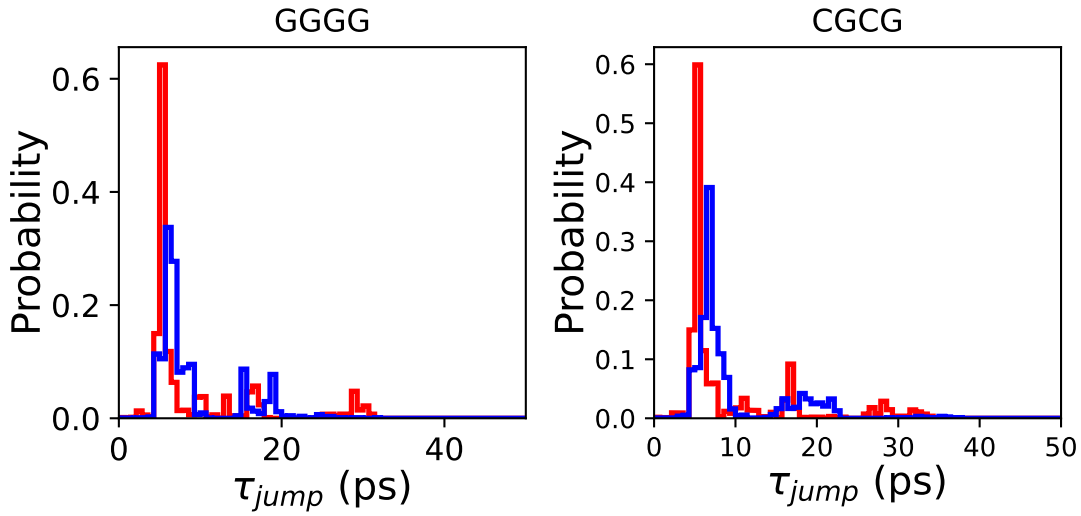

Figure S7: Jump time distributions for DNA (red) and RNA (blue) versions of the GGGG (left) and CGCG (right) sequences.

Different decompositions of the jump time distributions for the CGCG DNA and RNA sequences are shown in Figure S8, which is the analogous of Figure 2 in the main text (GGGG).

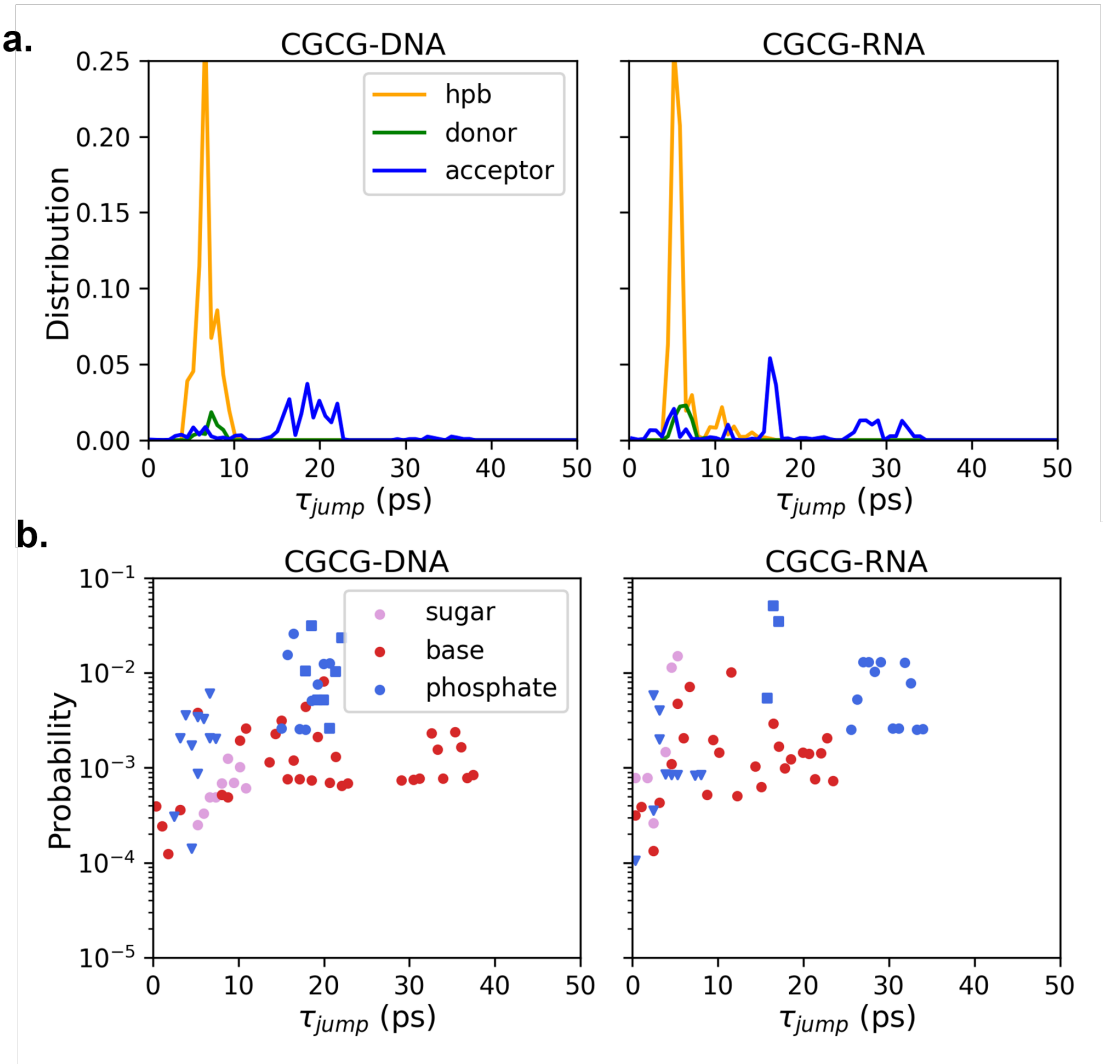

Figure S8: a) Distributions of jump time τ_{jump} for water molecules in the hydration shell of both DNA- and RNA- GGGG sequences, decomposed into contributions from water molecules assigned to hydrophobic sites ("hpb", orange), H-bond donor sites (green). b) Distributions of jump time τ_{jump} for water molecules H-bonded to acceptor sites in the hydration shell of both DNA- and RNA- GGGG sequences, decomposed into contributions from water molecules hydrating the sugar (pink), base (red), or phosphate (blue) moieties. Phosphate acceptors are further decomposed into O_R (squares), O_S (circles) and O3′ or O5′ (triangles) atoms. Plots were prepared using Matplotlib.[S35]

Site-resolved maps of jump times

Figure S9 shows the mapping of site-resolved jump times on the nucleic acid surface.

Focusing on the phosphate groups hydration in RNA, we investigated whether water molecules initially bridging two phosphate O_R atom have specific dynamics. To this aim, we

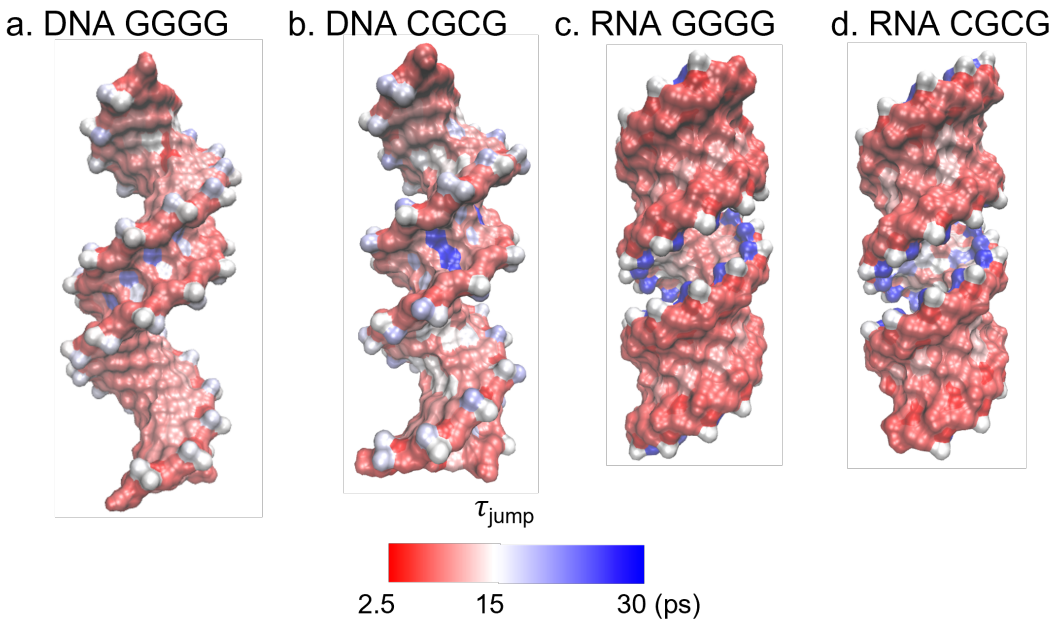

Figure S9: Maps of the site-resolved jump time τ_{jump} for water molecules in the hydration shell of a) DNA GGGG, b) DNA CGCG, c) RNA GGGG, and d) RNA CGCG sequences. Snapshots were prepared using the VMD software.[S23]

computed the jump TCF separately for water molecules initially H-bonded to a phosphate O_R atom depending on whether their second hydrogen atom is H-bonded to the O_R atom of the neighbor phosphate group (bridge conformation), or to water (not bridge) (Fig S10). These two populations exhibit very similar dynamics.

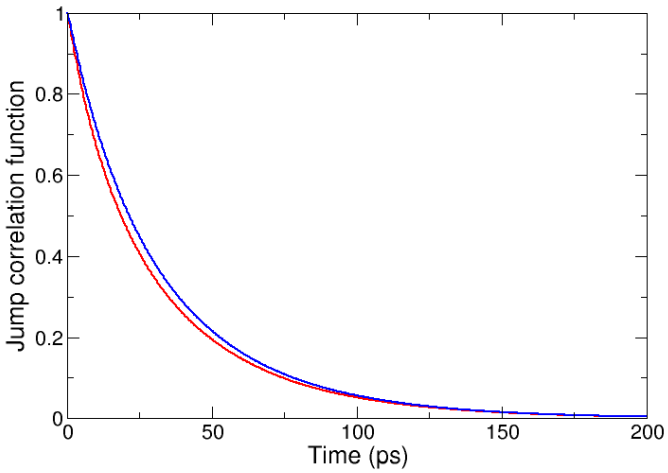

Figure S10: Jump TCF for water molecules initially H-bonded to a phosphate O_R atom depending on whether their second hydrogen atom is H-bonded to the O_R atom of the neighbor phosphate group (bridge conformation) (red), or to water (not bridge) (blue).

Analysis of phosphate hydration dynamics

H-bond lifetimes distributions

Previous works by Auffinger and Westhof,[S36–S38] reported very long residence times, of respectively 500 and 700 ps for phosphate O_S and O_R, two orders of magnitude slower than our jump times. This very slow reported timescale was defined as the longest H-bond lifetime observed during the simulation at a specific RNA site, which is fundamentally different from our jump time.

As the jumps follow Poisson statistics, we expect an exponential distribution of H-bond lifetimes at a given site with the jump time as characteristic timescale. Hence the longest H-bond lifetime, as previously noted,[S36–S38] depends on the overall simulation length.

The distribution of H-bond lifetimes (defined as the time between two jumps) for a given O_R site is depicted Figure S11a. While most of the water molecules form only short-lived H-bonds at this site, the distribution exhibits an extremely long tail that extends up to over 300 ps. The jump time for this site is $\tau_{jump} = 29.8$ ps. Figure S11b compares the H-bond

lifetime distributions for all phosphate O_R and O_S sites of the RNA GGGG system. As expected again, while most of the H-bond have very short lifetimes, we can find rare events of much longer-lived H-bonds, up to almost 600ps for O_R. Long-lived H-bonds are more probable at O_R than O_S sites, as expected since the characteristic timescale for the jump is longer at O_R than O_S, and the jump probability decreases as $\exp(-t/\tau_{jump})$.

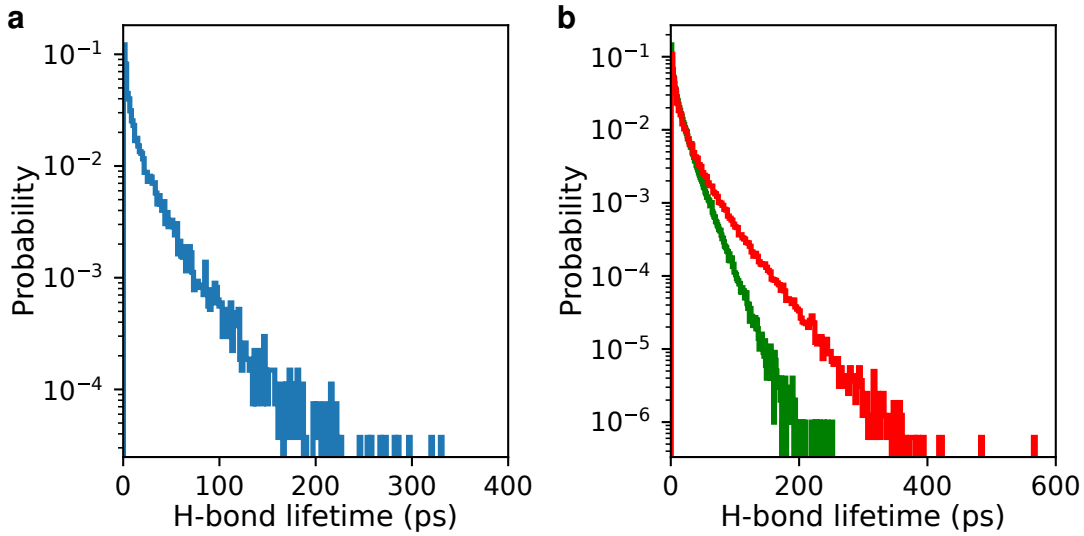

Figure S11: a) Distribution of computed H-bond lifetimes at a given phosphate O_R site in our RNA GGGG simulation. b) Distribution of computed H-bond lifetimes for all phosphate O_R and O_S sites in the same simulation.

Phosphate hydration dynamics rationalized with the Extended Jump Model

Table S2 allows to identify the origin of the difference between the phosphate O_R and O_S hydration dynamics— quantified with the ratio $\langle\rho\rangle_R/\langle\rho\rangle_S$— by examining how this ratio is predicted with different ingredients of the extended jump model (ρ_{TSEV}, ρ_{TSHB},...)

Table S2: Ratio $\langle\rho\rangle_R/\langle\rho\rangle_S$ (which reports on the split between the phosphate O_R and O_S hydration dynamics), computed either directly from the observed jump times, or from different ingredients of the Extended Jump Model: TSEV with/without ions, TSHB, TSEV$\times$ TSHB ; for DNA-GGGG and RNA-GGGG.

	ρ_{jump}	ρ_{TSEV}	ρ_{TSEV}^{ions}	ρ_{TSHB}	$\rho_{TSEV} \times \rho_{TSHB}$	$\rho_{TSEV}^{ions} \times \rho_{TSHB}$
DNA	0.83	0.93	0.93	0.86	0.80	0.80
RNA	1.73	1.26	1.38	1.17	1.46	1.61

Figure S12 illustrates the typical localization of water molecules H-bonded to O_R in RNA, in a confined space between the groove and the phosphate group pointing towards it, which is consistent with the high computed TSEV.

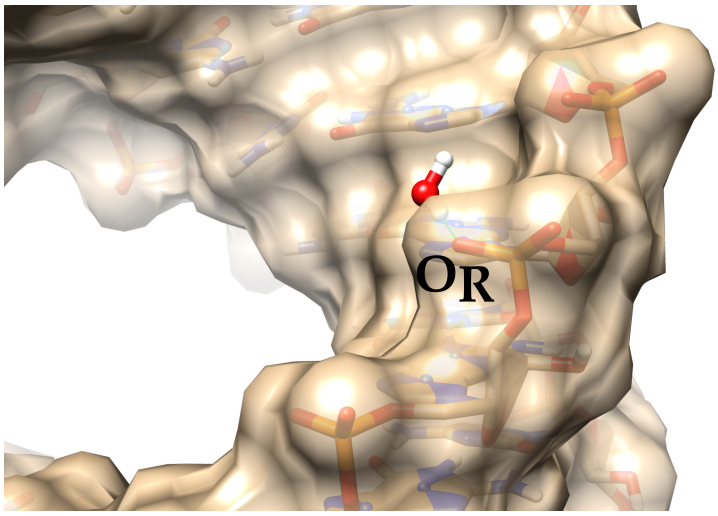

Figure S12: Typical arrangement of a water molecule H-bonded to the phosphate O_R atom in RNA.

Geometric analysis of phosphate orientation

To quantify the difference in orientation of the phosphate group with respect to the grooves in the DNA and RNA sequences, we evaluated several quantities. First, after the alignment

of all the snapshot along the principal z-axis, we computed the angles α_{OP2}, α_{P_S} and α_{P_R}, as described and defined in Fig. 4 of the main text. The angle α_{OP2} allows to determine the orientation of the phosphate group with respect to the z-axis. The angles α_{P_S} and α_{P_R} are related to the orientation of OP_S and OP_R with respect to the grooves. In other words, these angles allow to quantify if OP_S and/or OP_R point inside ($\alpha_{Pi} < 90°$) or outside the groove. We observed that the phosphate group is more parallel to the z-axis for the RNA duplexes (see Figure 4). In fact, the average values of α_{OP2} are between 29.7° and 36.4° and between 28.3° and 37.3° for GGGG-RNA and CGCG-RNA respectively, when on the contrary they are between 48.8° and 66.5° and between 62.0° and 70.1° for GGGG-DNA and CGCG-DNA respectively. By evaluating the mean values of the angles α_{P_S} and α_{P_R} (see Figure S6),in DNA duplexes O2P always points outside the groove (average values of α_{P_R} between 146.4° and 160.4° and between 136.9° and 151.9° for for GGGG-DNA and CGCG-DNA respectively) and OP_S sometimes slightly points inside the groove (average values of α_{P_S} between 70.3° and 87.3° and between 84.8° and 97.9° for for GGGG-DNA and CGCG-DNA respectively), when in RNA duplexes $\mathrm{O}P_S$ always points outside the groove (average values of α_{P_S} between 130.9° and 142.7° and between 134.2° and 144.8° for for GGGG-RNA and CGCG-RNA respectively) and OP_R always points inside the groove (average values of α_{P_R} between 20.7° and 55.1° and between 28.9° and 51.9° for for GGGG-RNA and CGCG-RNA respectively).

Ion density maps

The K^+ ion density around DNA and RNA GGGG 18-mers is shown on Figure S13. The narrow major groove in RNA and the associated short distance between the phosphate groups on both sides of the groove lead to a much higher concentration of ions next to the phosphate groups than in DNA. The full density maps have been deposited in the Zenodo folder[S21] to allow for more in-depth analysis of ion locations, which is beyond the scope of the present work.

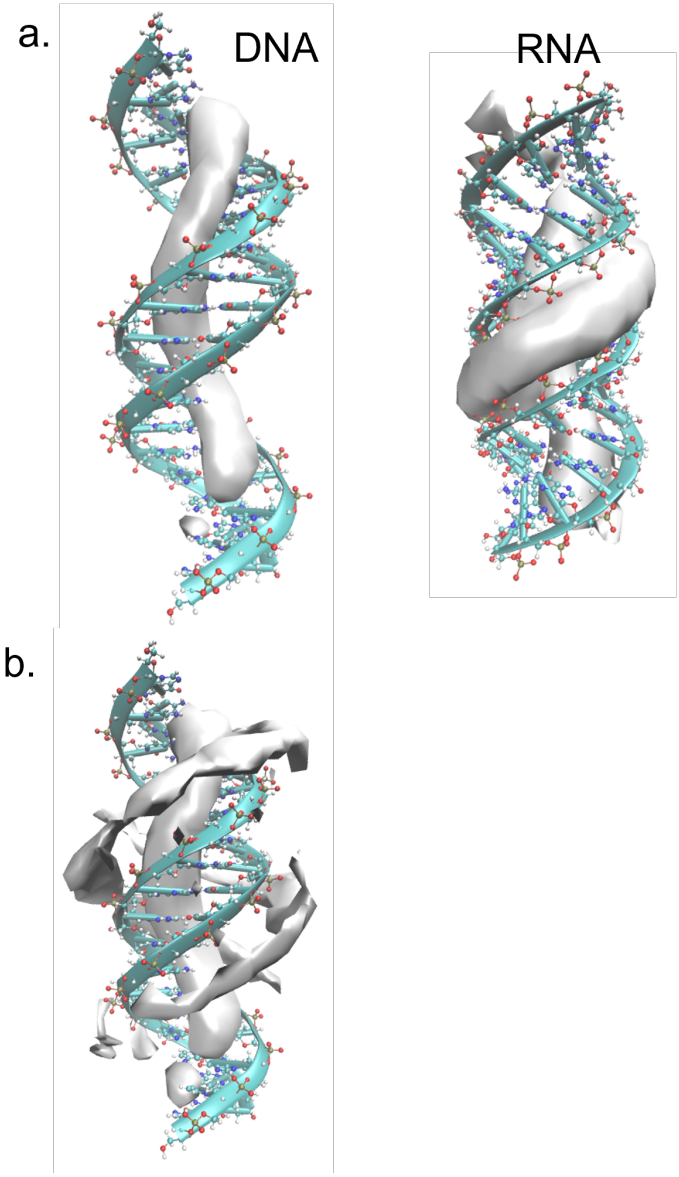

Figure S13: a) K^+ ion density maps around DNA (left) and RNA (right) at the same ion density cutoff. b) K^+ ion density maps around DNA at half the density cutoff used in a.

The decay of the jump correlation function is found independent of the initial presence in the first two hydration shells of the considered water molecule of a potassium ion (Figure S14).

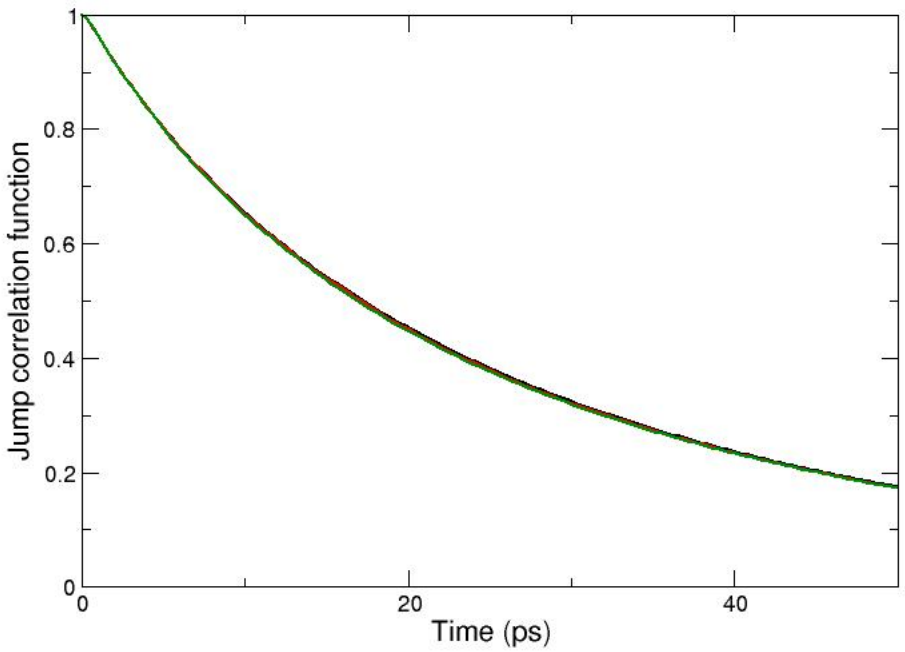

Figure S14: Jump correlation function averaged over all O_R phosphate sites in GGGG-RNA, depending on the absence (black) or presence at the time origin of a K^+ ion in the first (red) or second (green) hydration shell.

Analysis of the hydration dynamics at slow sites associated with bases inside the narrow groove

The location of the O2(C) sites, that exhibit the slowest hydration dynamics in DNA but much faster in RNA, is shown on Figure S15. Table S3 summarizes the average value of the jump retardation factor computed at those sites, from our simulation, and with our analytic jump model, with the two components TSEV and TSHB. In these confined locations, the jump models fails to predict the overall jump retardation, but still captures the larger slowdown in DNA than RNA. The failure of the jump models here is not suprising because it is meant to predict the jump time to bulk water, whereas about half of the jumps (65% in DNA and 45% in RNA) occur towards another acceptor of the biomolecule (instead of water). It is interesting to note that in RNA, even if the site is less confined (smaller TSEV),

proportionally more jumps occur towards another DNA site (mainly N3(G)) rather than to a water molecule. This may be because the N3 atom is slightly closer to O2 in the B-form helix than in the A-helix.

We also note that acceptor sites in the RNA deep groove, G(O6), also have a fast hydration dynamics ($\rho_{jump} = 3.2$) and a low TSEV retardation factor ($\rho_{TSEV} = 7.4$), much smaller than for O2 sites in the shallow grooves. This shows that even if the RNA deep groove is very narrow (more so than the DNA minor groove), what matters for hydration dynamics is the very local steric hindrance rather than larger scale features of the double helix.

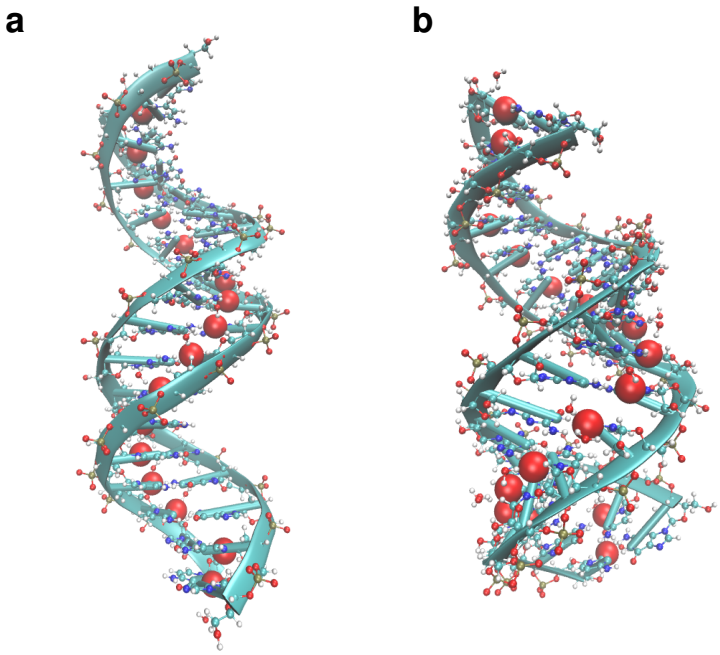

Figure S15: a) ds-DNA and b) ds-RNA GGGG systems, with the location of O2(C) sites in red balls, together with water molecules H-bonded to these sites.

Table S3: Average jump retardation factor directly computed from our simulations ρ_{jump}, average TSEV and TSHB retardation factors predicted from our jump model averaged over the O2(C) sites of the 14 central base pairs.

	ρ_{jump}	ρ_{TSEV}	ρ_{TSHB}
RNA	3.8	33.1	2.1
DNA	10.5	46.4	4.9

References

(S1) Lavery, R.; Zakrzewska, K.; Sklenar, H. JUMNA (Junction Minimisation of Nucleic Acids). *Comput. Phys. Commun.* **1995**, *91*, 135–158.

(S2) Pérez, A.; Marchán, I.; Svozil, D.; Sponer, J.; Cheatham, T. E.; Laughton, C. A.; Orozco, M. Refinement of the AMBER Force Field for Nucleic Acids: Improving the Description of α/γ Conformers. *Biophys. J.* **2007**, *92*, 3817–3829.

(S3) Tsui, V.; Case, D. A. Theory and Applications of the Generalized Born Solvation Model in Macromolecular Simulations. *Biopolymers* **2000**, *56*, 275–291, Publisher: John Wiley & Sons, Inc.

(S4) Hess, B.; Kutzner, C.; Van Der Spoel, D.; Lindahl, E. GROMACS 4: Algorithms for Highly Efficient, Load-Balanced, and Scalable Molecular Simulation. *J. Chem. Theory Comput.* **2008**, *4*, 435–447.

(S5) Van Der Spoel, D.; Lindahl, E.; Hess, B.; Groenhof, G.; Mark, A. E.; Berendsen, H. J. C. GROMACS: Fast, Flexible, and Free. *J. Comput. Chem.* **2005**, *26*, 1701–1718.

(S6) Lindahl, E.; Hess, B.; Van Der Spoel, D. GROMACS 3.0: A Package for Molecular Simulation and Trajectory Analysis. *J. Mol. Mod.* **2001**, *7*, 306–317.

(S7) Pronk, S.; Páll, S.; Schulz, R.; Larsson, P.; Bjelkmar, P.; Apostolov, R.; Shirts, M. R.; Smith, J. C.; Kasson, P. M.; van der Spoel, D.; Hess, B.; Lindahl, E. GROMACS 4.5: A High-Throughput and Highly Parallel Open Source Molecular Simulation Toolkit. *Bioinformatics* **2013**, *29*, 845–854.

(S8) Zgarbová, M.; Otyepka, M.; Šponer, J.; Mládek, A.; Banáš, P.; Cheatham, T. E.; Jurečka, P. Refinement of the Cornell et Al. Nucleic Acids Force Field Based on Reference Quantum Chemical Calculations of Glycosidic Torsion Profiles. *J. Chem. Theory Comput.* **2011**, *7*, 2886–2902.

(S9) Berendsen, H. J. C.; Grigera, J. R.; Straatsma, T. P. The Missing Term in Effective Pair Potentials. *J. Phys. Chem.* **1987**, *91*, 6269–6271.

(S10) Schmidt, J. R.; Roberts, S. T.; Loparo, J. J.; Tokmakoff, A.; Fayer, M. D.; Skinner, J. L. Are Water Simulation Models Consistent with Steady-State and Ultrafast Vibrational Spectroscopy Experiments? *Chemical Physics* **2007**, *341*, 143–157.

(S11) Duboué-Dijon, E.; Fogarty, A. C.; Hynes, J. T.; Laage, D. Dynamical Disorder in the DNa Hydration Shell. *J. Am. Chem. Soc.* **2016**, *138*, 7610–7620.

(S12) Kuhrova, P.; Otyepka, M.; Sponer, J.; Banáš, P. Are Waters Around RNA More Than Just a Solvent?–an Insight from Molecular Dynamics Simulations. *J. Chem. Theory Comput.* **2014**, *10*, 401–411.

(S13) Joung, I. S.; Cheatham III, T. E. Determination of Alkali and Halide Monovalent Ion Parameters for Use in Explicitly Solvated Biomolecular Simulations. *J. Phys. Chem. B* **2008**, *112*, 9020–9041.

(S14) Darden, T.; York, D.; Pedersen, L. Particle Mesh Ewald: An N Log (N) Method for Ewald Sums in Large Systems. *J. Chem. Phys.* **1993**, *98*, 10089–10092.

(S15) Essmann, U.; Perera, L.; Berkowitz, M. L.; Darden, T.; Lee, H.; Pedersen, L. G. A Smooth Particle Mesh Ewald Method. *J. Chem. Phys.* **1995**, *103*, 8577–8593.

(S16) Hess, B.; Bekker, H.; Berendsen, H. J. C.; Fraaije, J. G. E. M. LINCS: A Linear Constraint Solver for Molecular Simulations. *J. Comput. Chem.* **1997**, *18*, 1463–1472.

(S17) Harvey, S. C.; Tan, R. K.-Z. . Z.; Cheatham, T. E. The Flying Ice Cube: Velocity Rescaling in Molecular Dynamics Leads to Violation of Energy Equipartition. *J. Comput. Chem.* **1998**, *19*, 726–740.

(S18) Bussi, G.; Donadio, D.; Parrinello, M. Canonical Sampling Through Velocity Rescaling. *J. Chem. Phys.* **2007**, *126*, 14101.

(S19) Berendsen, H. J.; Postma, J. P. M. v.; van Gunsteren, W. F.; DiNola, A.; Haak, J. R. Molecular Dynamics with Coupling to an External Bath. *J. Chem. Phys.* **1984**, *81*, 3684–3690.

(S20) Parrinello, M.; Rahman, A. Polymorphic Transitions in Single Crystals: A New Molecular Dynamics Method. *J. Applied Phys.* **1981**, *52*, 7182–7190.

(S21) Zenodo Dataset DOI:10.5281/Zenodo.10647894.

(S22) Lavery, R.; Moakher, M.; Maddocks, J. H.; Petkeviciute, D.; Zakrzewska, K. Conformational Analysis of Nucleic Acids Revisited: Curves+. *Nucleic Acids Res.* **2009**, *37*, 5917–5929.

(S23) Humphrey, W.; Dalke, A.; Schulten, K. VMD: Visual Molecular Dynamics. *J. Mol. Graphics* **1996**, *14*, 33–38.

(S24) Pasi, M.; Maddocks, J. H.; Beveridge, D.; Bishop, T. C.; Case, D. A.; Cheatham, I., Thomas; Dans, P. D.; Jayaram, B.; Lankas, F.; Laughton, C.; Mitchell, J.; Osman, R.; Orozco, M.; Pérez, A.; Petkevičiūtė, D.; Spackova, N.; Sponer, J.; Zakrzewska, K.; Lavery, R. μABC: A Systematic Microsecond Molecular Dynamics Study of Tetranucleotide Sequence Effects in B-DNA. *Nucleic Acids Res.* **2014**, *42*, 12272–12283.

(S25) Frezza, E.; Courban, A.; Allouche, D.; Sargueil, B.; Pasquali, S. The Interplay Between Molecular Flexibility and RNA Chemical Probing Reactivities Analyzed at the Nucleotide Level Via an Extensive Molecular Dynamics Study. *Methods* **2019**, *162-163*, 108–127.

(S26) Fogarty, A. C.; Laage, D. Water Dynamics in Protein Hydration Shells: the Molecular Origins of the Dynamical Perturbation. *J. Phys. Chem. B* **2014**, *118*, 7715–7729.

(S27) Duboué-Dijon, E.; Laage, D. Comparative Study of Hydration Shell Dynamics Around a Hyperactive Antifreeze Protein and Around Ubiquitin. *J. Chem. Phys.* **2014**, *141*, 22D529.

(S28) Laage, D.; Hynes, J. T. A Molecular Jump Mechanism of Water Reorientation. *Science* **2006**, *311*, 832–835.

(S29) Laage, D.; Stirnemann, G.; Sterpone, F.; Rey, R.; Hynes, J. T. Reorientation and Allied Dynamics in Water and Aqueous Solutions. *Annu. Rev. Phys. Chem.* **2011**, *62*, 395–416.

(S30) Laage, D.; Hynes, J. T. On the Molecular Mechanism of Water Reorientation. *J. Phys. Chem. B* **2008**, *112*, 14230–14242.

(S31) https://hartree.chimie.ens.fr/waterdynamics/dnarna_hydration_dynamics.

(S32) Laage, D.; Stirnemann, G.; Hynes, J. T. Why Water Reorientation Slows Without Iceberg Formation Around Hydrophobic Solutes. *J. Phys. Chem. B* **2009**, *113*, 2428–2435.

(S33) Sterpone, F.; Stirnemann, G.; Hynes, J. T.; Laage, D. Water Hydrogen-Bond Dynamics Around Amino Acids: The Key Role of Hydrophilic Hydrogen-Bond Acceptor Groups. *J. Phys. Chem. B* **2010**, *114*, 2083–2089.

(S34) Inc., T. M. MATLAB Version: 9.13.0 (R2022a). The MathWorks Inc., 2022.

(S35) Hunter, J. D. Matplotlib: a 2D Graphics Environment. *Comput. Sci. Eng.* **2007**, *9*, 90–95.

(S36) Auffinger, P.; Westhof, E. Water and Ion Binding Around RNA and DNA (C,G) Oligomers. *J. Mol. Biol.* **2000**, *300*, 1113–1131.

(S37) Auffinger, P.; Westhof, E. RNA Hydration: Three Nanoseconds of Multiple Molecular Dynamics Simulations of the Solvated tRNA(Asp) Anticodon Hairpin. *J. Mol. Biol.* **1997**, *269*, 326–341.

(S38) Auffinger, P.; Westhof, E. Water and Ion Binding Around R(UpA)12 and D(TpA)12 Oligomers - Comparison with RNA and DNA (CpG)12 Duplexes. *J. Mol. Biol.* **2001**, *305*, 1057–1072.